coatings

MDPI

Article

Surface Modification of Nano-Al_2O_3 with Silane Coupling Agent and Its Effect on the Compressive Strength of PI/Al_2O_3 Composites

Jing Cao [1,†], Yu Wang [1,†], Guanghua Liu [2], Qingyuan Shang [1], Bicheng Wang [1], Jian Sun [2], Yu Bai [1,*], Ming Liu [3], Fangli Yu [4,*], Guozheng Ma [3] and Haidong Wang [3]

1 State Key Laboratory for Mechanical Behavior of Materials, Xi'an Jiaotong University, Xi'an 710049, China; cj161124@stu.xjtu.edu.cn (J.C.); wangyu0730@mail.xjtu.edu.cn (Y.W.); sqy13619219329@stu.xjtu.edu.cn (Q.S.); wbcxjtu@stu.xjtu.edu.cn (B.W.)
2 China United Gas Turbine Technology Co., Ltd., Beijing 102209, China; zdxjtu@stu.xjtu.edu.cn (G.L.); 18438603117@163.com (J.S.)
3 National Key Lab for Remanufacturing, Army Academy of Armored Forces, Beijing 100072, China; 15383255791@163.com (M.L.); magz0929@163.com (G.M.); whaidou2021@163.com (H.W.)
4 School of Materials Engineering, Xi'an Aeronautical University, Xi'an 710077, China
* Correspondence: byxjtu@mail.xjtu.edu.cn (Y.B.); 201607046@xaau.edu.cn (F.Y.)
† These authors contributed equally to this work.

Abstract: In this study, a series of nano-Al_2O_3 reinforced polyimide (PI) composites were fabricated using the hot compression method. A silane coupling agent was used to modify the surface of nano-Al_2O_3 powder to enhance the PI/Al_2O_3 interface compatibility. The effects of Al_2O_3 contents on the microstructures, thermal behavior and mechanical properties of PI/Al_2O_3 composites were investigated. The results suggested that chemical reactions occurred during in situ modification. The nano-Al_2O_3 was cross-linked to the PI matrix, which reduced the mobility of PI chains and improved the elastic modulus of the composites. When the Al_2O_3 content was 30 wt.%, the compressive strength of composites reached the maximum value of 313 MPa and increased by 26.5% than that of the PI matrix.

Keywords: polyimide; Al_2O_3; composite; surface modification; compressive strength

check for updates

Citation: Cao, J.; Wang, Y.; Liu, G.; Shang, Q.; Wang, B.; Sun, J.; Bai, Y.; Liu, M.; Yu, F.; Ma, G.; et al. Surface Modification of Nano-Al_2O_3 with Silane Coupling Agent and Its Effect on the Compressive Strength of PI/Al_2O_3 Composites. *Coatings* **2024**, *14*, 27. https://doi.org/10.3390/coatings14010027

Academic Editor: Aivaras Kareiva

Received: 28 November 2023
Revised: 20 December 2023
Accepted: 20 December 2023
Published: 25 December 2023

1. Introduction

Polyimide (PI) has great potential in the field of flexible composite materials or microelectronic devices due to its excellent structural flexibility, biocompatibility, chemical stability and high dielectric constant [1–3]. In particular, aromatic polyimide, containing rigid imide and aromatic ring structures, is classified as a high-performance polymer owing to its excellent thermal and mechanical properties. Currently, PI is one of the best temperature-resistant materials in resin matrix composites and is considered one of the most potential materials to replace metal as structural components in the field of aerospace [4,5]. But, compared to metals and ceramics, the weak mechanical performance and low-temperature resistance greatly limit the application of PI. Therefore, it is of great importance to enhance its strength, modulus and thermal stability to broaden its development potential.

The results of a growing number of studies suggest the use of nanoparticles, such as boron nitride [6], alumina [7,8], carbon nanotubes [9], graphene oxide [10,11], silica [12,13] and layered silicate [14], can improve the mechanical properties, temperature resistance, flame retardancy, optics, wear resistance and dielectric properties of polymers [15–19]. Compared to the microparticles, the nanoparticles can achieve better performance with less addition owing to their large specific surface area [20]. Among these nanoparticles, nano-Al_2O_3 has a series of unique properties, such as good thermal conductivity, high strength, mechanical strength, wear resistance, thermal stability and electrical insulation.

Nevertheless, nano-Al_2O_3 has high surface activity and tends to form agglomerates or clusters in the polymer matrix. In addition, differences in hydrophobicity usually lead to poor interfacial interaction between Al_2O_3 and polymers, which consequently results in the degradation of mechanical properties. Therefore, it is necessary and important to modify the surface of nanoparticles to overcome their tendency to aggregate and improve their dispersion in the polymer matrix.

It is well known that grafting synthetic polymers is a useful approach for modifying the surface of nanoparticles. For instance, Belgacemi et al. [21] used the 3-aminopropyltrimethoxysilane (APS) coupling agent to modify the surface of nano-Al_2O_3 and prepared epoxy/oxidized ultrahigh molecular weight polyethylene (UHMWPE)/Al_2O_3 composites. The flexural modulus increased from 6.9 to 13.2 GPa, while the flexural strength increased by 25% to 159 MPa after adding 5 wt.% Al_2O_3. The hydrolysis of silane coupling agents produces silicon–oxygen bonds and hydroxide ions [22]. Duan et al. [23] used three coupling agents to surface modify nano-Al_2O_3, including 3-aminopropyltriethoxysilane (KH550), γ-methacryloyloxypropyltrimethoxysilane (KH570) and tetraisopropyl di(dioctylphosphate) titanate (NDZ401). The results on the DC electrical properties of Al_2O_3/low-density polyethylene (LDPE) composites revealed that surface modification significantly affected their properties. However, there are only a few studies on the compressive properties of PI-based composites reinforced using nano-Al_2O_3. In addition, due to the high surface energy of nanoparticles, the content of nanoparticles was usually less than 10%.

Based on the above background, aromatic polyimide and nano-Al_2O_3 powders were used to prepare PI/Al_2O_3 composites. The silane coupling agent was used to modify the surface of nano-Al_2O_3 with the aim of enhancing the PI/Al_2O_3 interface compatibility in the present work. The PI-based composites with different Al_2O_3 contents were fabricated using the hot-pressing method and post-heat treatment. The effects of Al_2O_3 content and surface modification on the compressive strength of PI were elaborated. In addition, the thermal behaviors of PI were investigated using differential scanning calorimetry.

2. Materials and Experimental Procedures

2.1. Materials and Surface Modification of Nano Al_2O_3

The PI and Al_2O_3 powder (Beijing Sunspraying New Material Co., Ltd., Beijing, China) were used in the preparation of composite materials. The molecular weight and intrinsic viscosity of polyimide were 30,000 and 0.5–0.7 dL/g, respectively. The specific surface area and particle size distribution of Al_2O_3 were 230 m^2/g and 20–50 nm, respectively. Figure 1 shows the synthesis of polyimide as well as the crosslinked products. The schematic diagram of the surface modification of Al_2O_3 with 3-aminopropyltriethoxysilane (KH550) silane coupling agent (≥99.0%, Shanghai Macklin Biochemical Co., Ltd., Shanghai, China) is shown in Figure 2. As shown in Figure 2, the Al_2O_3 particle was dried at 100 °C for 12 h to remove surface adsorbents, and then ultrasonically dispersed for 30 min by adding Al_2O_3 to an ethanol solution. The silane coupling agent was added to the mixed solution of ethanol and water. The mass ratio of the coupling agent, ethanol and water was 20:72:8. Furthermore, acetic acid (Sinopharm Chemical Reagent Co., Ltd. Shanghai, China) was added to adjust the pH to 4. The acidic media improved the hydrolysis reaction, and the resultant silanol was very stable. And, the solution was hydrolyzed with ultrasound for 30 min. Then, the mixture of Al_2O_3 powder and silane coupling agent was stirred for 4 h at 80 °C. The mass ratio of the silane coupling agent and Al_2O_3 was 1 to 20. The degree of silane grafting was characterized through differential scanning calorimetry (DSC). The DSC method easily reflected the weight loss, especially the loss of organic polymer at high temperatures. In this paper, the silane coupling agent belonged to the organic polymer. The surface grafting-modified Al_2O_3 using a silane coupling agent will decompose and experience weight loss after high-temperature treatment. The loss value meant a decrease in silane grafting. Therefore, the difference in weight loss between the modified Al_2O_3 and the unmodified Al_2O_3 was the grafting specific gravity of the coupling agent. Figure 3 shows the TGA results of the original and modified Al_2O_3. The weight loss of nanoparticles

<100 °C was mainly due to water desorption. The weight loss between 100 and 800 °C was mainly caused by the loss of organic groups grafted on the nanoparticle surface [23]. For the original Al_2O_3 powder, the total loss was 4.1%, and this is due to the loss of absorbed moisture. And the weight loss was up to 8.3% for modified Al_2O_3 powder. Thus, the grafting rate of Al_2O_3 after modification was 4.2 wt.%.

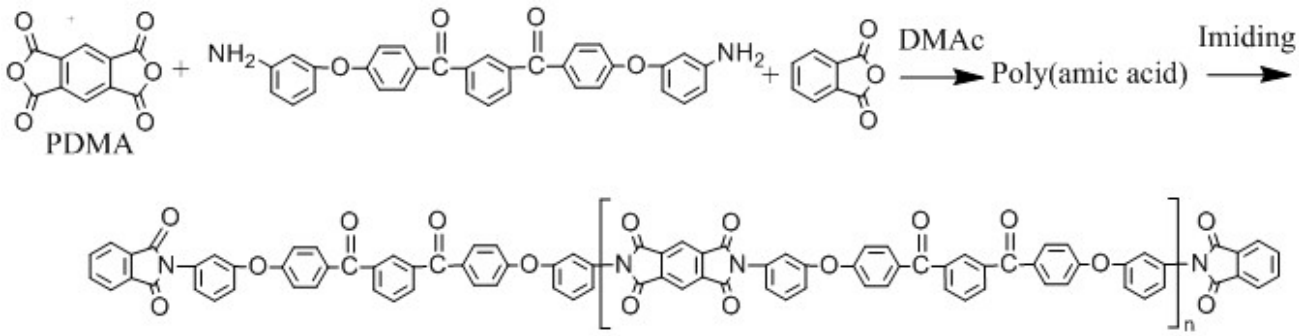

Figure 1. Synthesis of polyimide [4].

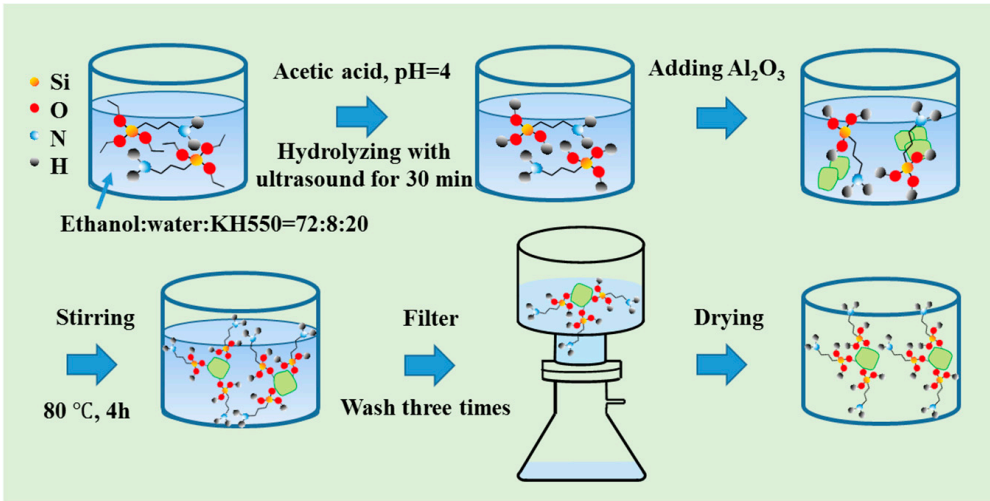

Figure 2. Schematic diagram of surface modification of nano-Al_2O_3 using a silane coupling agent.

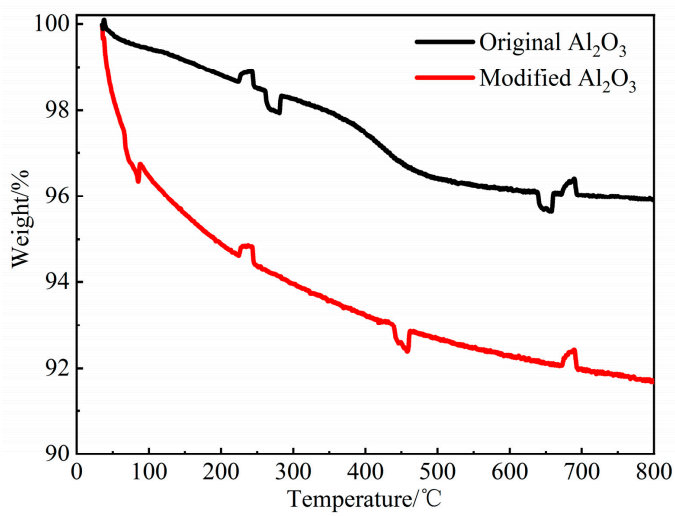

Figure 3. TGA curves of original and modified Al_2O_3.

2.2. Preparation of PI/Al_2O_3 Composites

The PI and surface-modified Al_2O_3 powders were stirred and mixed in a high-speed mechanical mixer at 2000 rpm for 30 min. The compositions of Al_2O_3/PI composites are listed in Table 1. The preparation process was divided into two stages: The first stage was hot pressing, and then the mixture was dispersed and pressed for 30 min under a pressure of 100 MPa at 220 °C. The second stage was post-treatment, conducted in three steps: first at 180 °C for 1 h, then at 200 °C for 1 h, and finally at 230 °C for 4 h.

Table 1. Samples and compositions of PI/Al_2O_3 composites.

Samples	PI/wt.%	Al_2O_3/wt.%	Modified through KH550 Silane Coupling Agent
PI	100	0	No
10 A	90	10	No
20 A	80	20	No
30 A	70	30	No
40 A	60	40	No
50 A	50	50	No
10 A-K	90	10	Yes
20 A-K	80	20	Yes
30 A-K	70	30	Yes
40 A-K	60	40	Yes
50 A-K	50	50	Yes

2.3. Microstructural Characterization, Thermal Stability and Mechanical Properties

The interface of composites was observed using scanning electron microscopy (SEM, SU3500, Timei Scientific Instrument Co., Ltd., Shanghai, China) and transmission electron microscopy (TEM, JEM-2100, JEOL Japan Electronics Co., Ltd., Tokyo, Japan). Differential scanning calorimetry (DSC) was performed on METTLER TOLEDO TGA/DSC3+ (METTLER TOLEDO, Ltd., Shanghai, China) under a nitrogen atmosphere. The composites were heated up to 800 °C at a rate of 10 °C/min. Crystalline structures of both PI and Al_2O_3 powders were characterized using X-ray diffraction (XRD, D8 DVANCE, Bruker Technology Co. Ltd., Karlsruhe, Germany) with Cu Ka radiation (1.5406 nm) using a 0.008° step size, 8°/min scanning speed, 45 kV tube voltage, 40 mA tube current, and diffraction angle from 10 to 90°. The peak fitting of XRD patterns was carried out using MDI Jade 6.0 software. Fourier transform infrared spectroscopy (FTIR) was performed using a Micro-Infrared Spectroscopy (Bruker VERTEX70) covering the range from 4000 to 400 cm^{-1} to evaluate the structure of surface-functionalized nano-Al_2O_3. X-ray photoelectron spectrometry (XPS, Thermo Fisher ESCALAB Xi+, Thermo Fisher Scientific, Waltham, MA, USA) was used to analyze the chemical composition of samples. The compressive strength of all composites was measured using a universal tensile testing machine (WDW-100KN, Ningbo Dexun Testing Equipment Co., Ltd., Ningbo, China) with a constant load rate of 1 mm/min. Three samples of each composition were tested to ensure repeatability and an average value was recorded. The roughness of the fracture surface was measured using a surface roughness measuring instrument (TR200, Shanghai Gaozhi Precision Instrument Co., Ltd., Shanghai, China). The porosity was estimated using Archimedes' principle (water displacement). In the Archimedean method, samples used for compression testing were used to measure porosity. The samples were cleaned and dried. The mass of corresponding samples was recorded as M_3. Then, the samples can be operated by pumping in distilled water for 5–7 h to facilitate pore penetration. This mass was recorded as M_2. Subsequently, the floating mass was measured in distilled water and recorded as M_1. Based on the equal volumes of the Archimedean principle ($\rho_0 gV = (M_2 - M_1)g$), the P was calculated using the following equation:

$$P = (M_2 - M_3)/(M_2 - M_1). \quad (1)$$

3. Results

3.1. Thermal Stability of PI/Al_2O_3 Composites

DSC analysis was conducted to investigate the thermal behavior of PI/Al_2O_3 composites. The heat flow density curves of PI powder and hot-pressed PI and the weight loss curves of PI/Al_2O_3 composites are demonstrated in Figure 4. It can be seen from Figure 4a that there is an exothermic peak on the heat flow density curve of the PI powder. The appearance of a peak at 230 °C indicates the occurrence of cross-linking reactions [24,25]. As seen from the heat flow density curve of the hot-pressed PI, the T_g of the hot-pressed PI material was 356.5 °C. In the weight loss curves shown in Figure 4b, it can be found that the thermal stability of the PI/Al_2O_3 composites improved after the addition of Al_2O_3, which hindered the transfer of heat. The temperature of 5% weight loss ($T_{5\%}$) of hot-pressed PI was 450.74 °C. And the thermal deposition temperature ($T_{5\%}$) of composites with 10 wt.%, 30 wt.% and 50 wt.% Al_2O_3 were 451 °C, 457.47 °C and 455.79 °C, respectively.

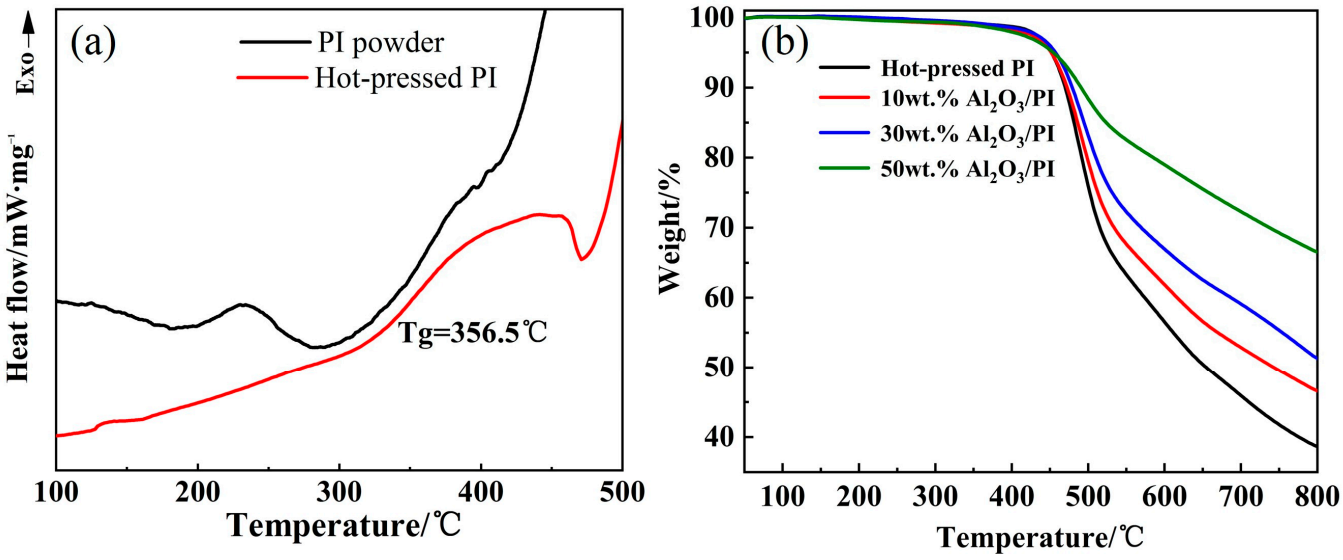

Figure 4. Heat flow density curves or weight loss curves of samples: (**a**) heat flow density curves of PI powder and hot-pressed PI; (**b**) weight loss curves of PI/Al_2O_3 composites fabricated through the hot-pressing method.

3.2. Surface Modification of Al_2O_3 Powder

Figure 5 depicts the morphologies and X-ray diffraction patterns of PI and Al_2O_3 powders. As shown in Figure 5a,b, the particle size of PI powder was approximately 2~10 μm and exhibited an irregular shape, while the size of Al_2O_3 powder ranged from 20 to 50 nm (see Figure 5d). Nano-Al_2O_3 particles are susceptible to agglomeration due to their high surface activity. The Al_2O_3 particles used are micron-scale particles formed through the agglomerate of nanoparticles in the SEM image (Figure 5c). And the particle size of undispersed particles was 2 to 10 μm. As shown in Figure 5e,f, the XRD pattern of PI powder exhibited only one broad peak and no sharp diffraction peaks corresponding to crystalline phases. In addition, XRD results of Al_2O_3 powder revealed that the phase structure consisted of the corundum and spinel phases (α-Al_2O_3 and γ-Al_2O_3).

Figure 6 shows the statistical results of the porosity of PI/Al_2O_3 composites with or without modified Al_2O_3 using the silane coupling agent, respectively. It can be seen from Figure 5 that the porosity of the composites slightly decreased after adding the modified Al_2O_3. The increased porosity had a close relationship with the agglomeration of nano-Al_2O_3. When the content of Al_2O_3 reached 50%, the porosity of the composites dramatically increased due to particle agglomeration. Figure 7 provides the fracture morphology of PI/Al_2O_3 composites. As shown in Figure 7, many Al_2O_3 particles accumulated in the PI matrix and formed a large number of pores, especially for the sample with 50% original

or modified Al_2O_3, which was harmful to the performance of the composites. It can be observed from Figure 7a–d that the agglomeration of Al_2O_3 was weakened to some extent after modification.

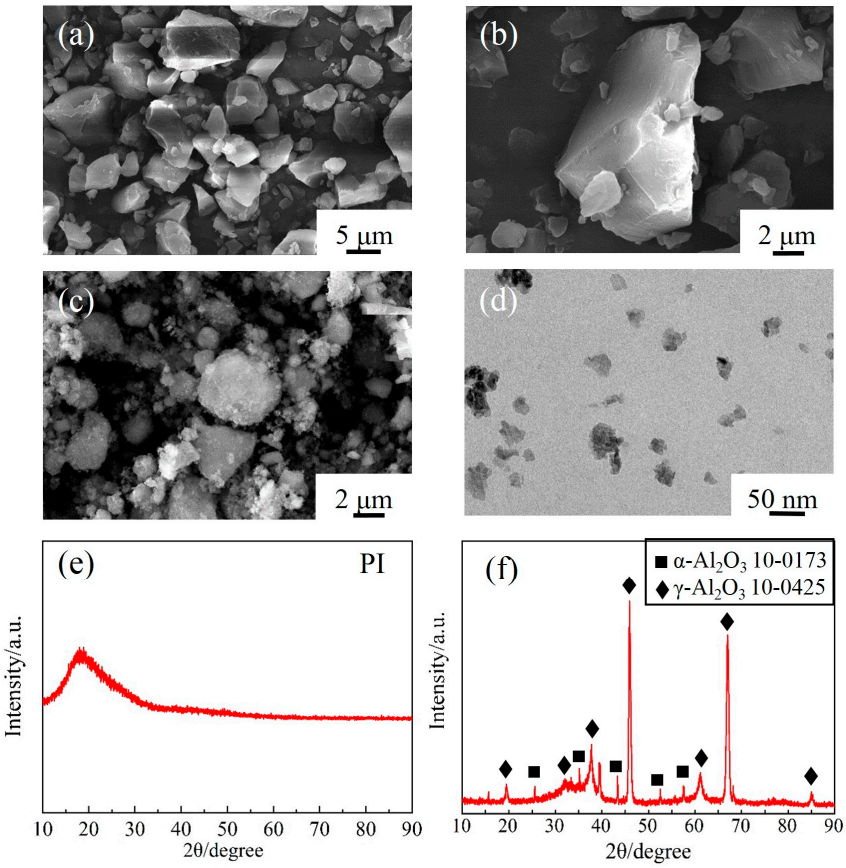

Figure 5. Morphology and X-ray diffraction (XRD) patterns of PI and original Al_2O_3 powders: (**a**) low magnification SEM image of PI powder; (**b**) high magnification SEM image of PI powder; (**c**) SEM image of Al_2O_3 powder; (**d**) TEM image of Al_2O_3 powder; (**e**) XRD pattern of PI powder; (**f**) XRD pattern of Al_2O_3 powder.

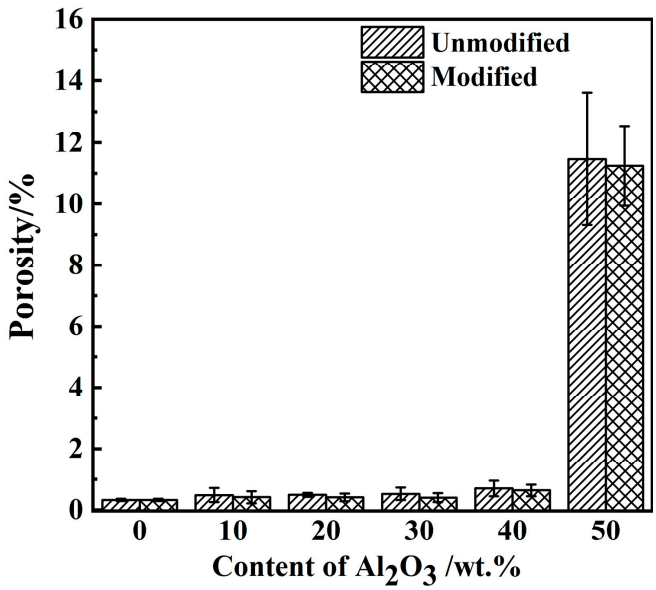

Figure 6. Porosity of PI/Al_2O_3 composites comprising unmodified and modified nano-Al_2O_3.

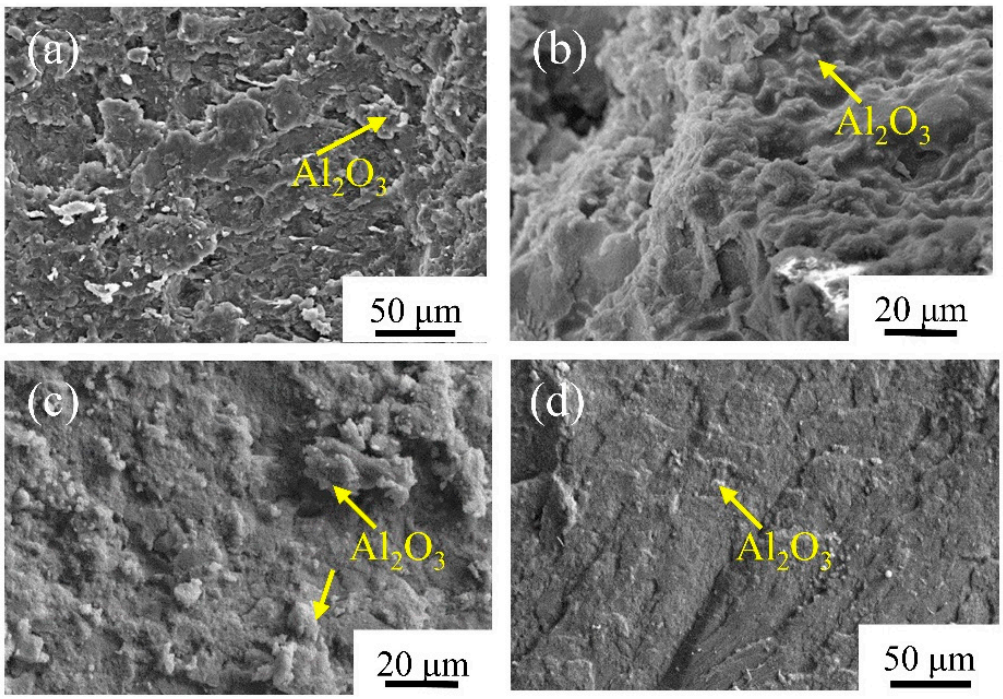

Figure 7. Fracture morphologies of PI/Al_2O_3 composites: (**a**) sample with 30 wt.% original Al_2O_3; (**b**) sample with 30 wt.% modified Al_2O_3; (**c**) sample with 50 wt.% original Al_2O_3; (**d**) sample with 50 wt.% modified Al_2O_3.

The hydrolyzed silane coupling agent reacted with the hydroxyl group on the surface of Al_2O_3 to form bonds, which can reduce the agglomeration of nano-Al_2O_3 and improve the interfacial compatibility with the polymer. The original and modified Al_2O_3 powders were characterized using FTIR and XPS to examine whether chemical reactions occurred during the in situ modification, and the results are shown in Figure 8. The Fourier transform infrared spectra of nano-Al_2O_3 are shown in Figure 8a,b. For the original Al_2O_3 powder, the peak at 1645 cm^{-1} corresponded to the bending vibration of O-H, and the peaks at 1075 cm^{-1}, 816 cm^{-1} and 746 cm^{-1} were the vibration of Al-O. After modification, some new peaks appeared, which corresponded to the bending vibration of -NH_2 and -CH_2- at 1570 and 1470 cm^{-1}, while 1431 cm^{-1} and 1053 cm^{-1} were the vibration peaks of Si-C-H and Al-O-Si, respectively. The vibration peak of -OH disappeared, and the vibration intensity of Al-O was significantly reduced. The emergence of new peaks of -NH_2, -CH_2-, Si-C-H and Al-O-Si suggested that the silane coupling agent was successfully coated on the surface of Al_2O_3 nanoparticles. The XPS results of the original and modified Al_2O_3 powders are shown in Figure 8c–f. It can be seen that the new peaks of N and Si appeared on the modified Al_2O_3, while C, Al and O were only present in the original one. Figure 9 exhibits the XRD patterns and the FTIR spectra of PI/Al_2O_3 composites with and without modified nano-Al_2O_3. After modification, the bonding of Al_2O_3 and PI was enhanced, and the amorphous peak strength of the polymer increased in XRD patterns. In the FTIR spectra, the peaks at 1380 cm^{-1}, 1730 cm^{-1} and 1780 cm^{-1} correspond to the stretching vibration peaks of C-N and C=O, respectively. The Si-O peak at 1100 cm^{-1} appeared in the composites with modified Al_2O_3. Additionally, the O-H peak decreased significantly, and the Al-O peaks at 815 cm^{-1} and 663 cm^{-1} decreased.

3.3. Mechanical Properties of PI/Al_2O_3 Composite Materials

The compression test was used to explore the effect of Al_2O_3 content and surface modification on the compressive strength of PI/Al_2O_3 composites. Figure 10 provides the compressive strength and modulus of PI/Al_2O_3 composites. As shown in Figure 10a, the compressive strength of the composites gradually increased with the increase of Al_2O_3

content. When the Al_2O_3 content was higher than 30 wt.%, the strength of the composites decreased due to the excessive filler content and uneven distribution of Al_2O_3 in the PI matrix. The compressive strength of composites with modified Al_2O_3 was higher than that of the original one. In addition, the composites with 30 wt.% Al_2O_3 exhibited the highest compressive strength for both of composites with or without modified Al_2O_3. The compressive strength of pure PI was 247.5 MPa. The compressive strength of composite with 30 wt.% Al_2O_3 was 313.0 MPa, and its compressive strength was 26.5% higher than pure PI. Similar to the results reported in previous studies, Sezavar et al. [26] found that the addition of 15 wt.% Al_2O_3 to PMMA caused an increase of approximately 25% in elastic modulus. From the compressive modulus shown in Figure 10b, it was found that the compressive modulus increased gradually with increasing the content of Al_2O_3. The compressive modulus increased after modification, while the composites with 40 wt.% Al_2O_3 exhibited the highest compressive modulus for both samples with modified or original Al_2O_3 powders.

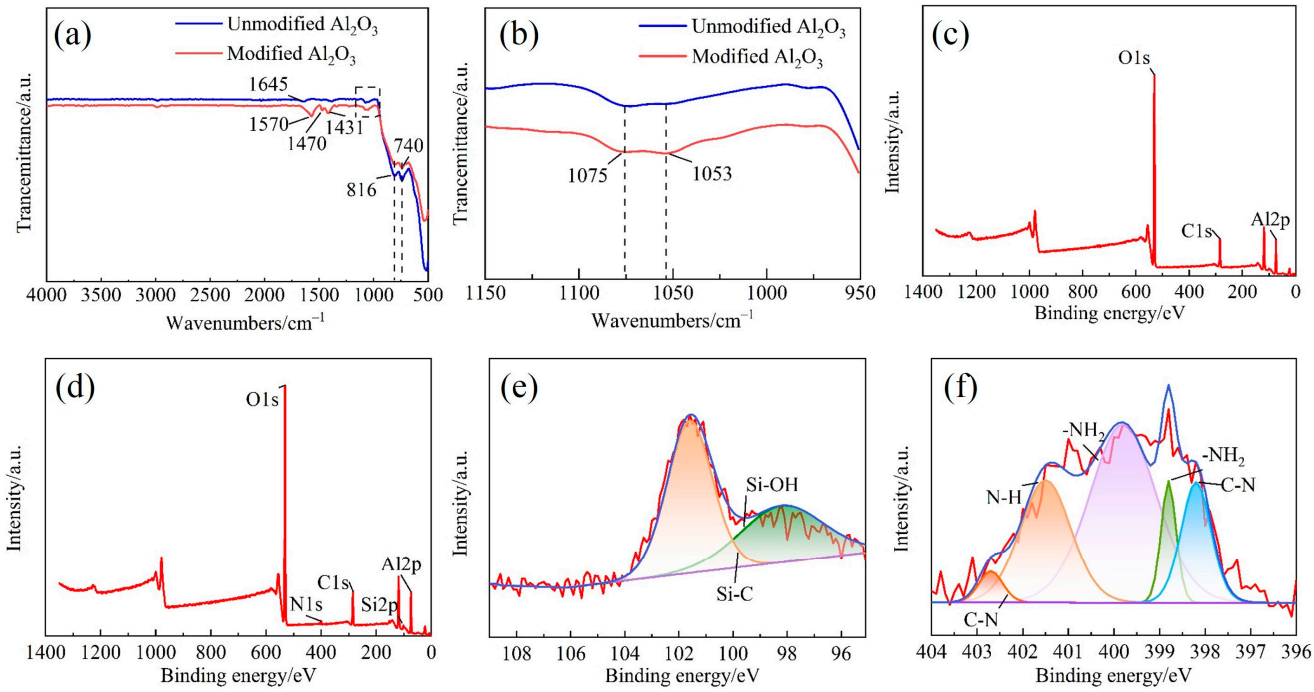

Figure 8. (**a**) FTIR spectrum of Al_2O_3; (**b**) local magnification; XPS spectrum of (**c**) survey scan of unmodified Al_2O_3; (**d**) survey scan of modified nano-Al_2O_3; (**e**) Si2p and (**f**) N1s of modified Al_2O_3.

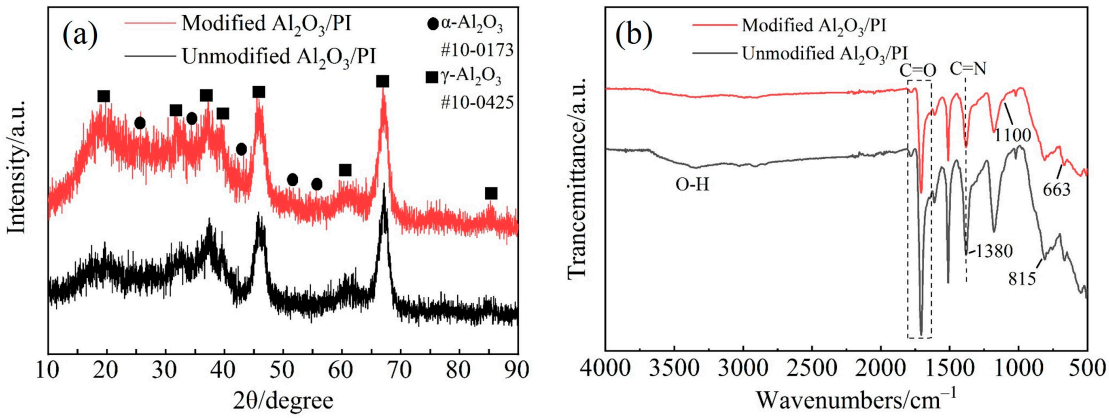

Figure 9. (**a**) XRD patterns and (**b**) FTIR spectra of PI/Al_2O_3 composites with and without modified nano-Al_2O_3.

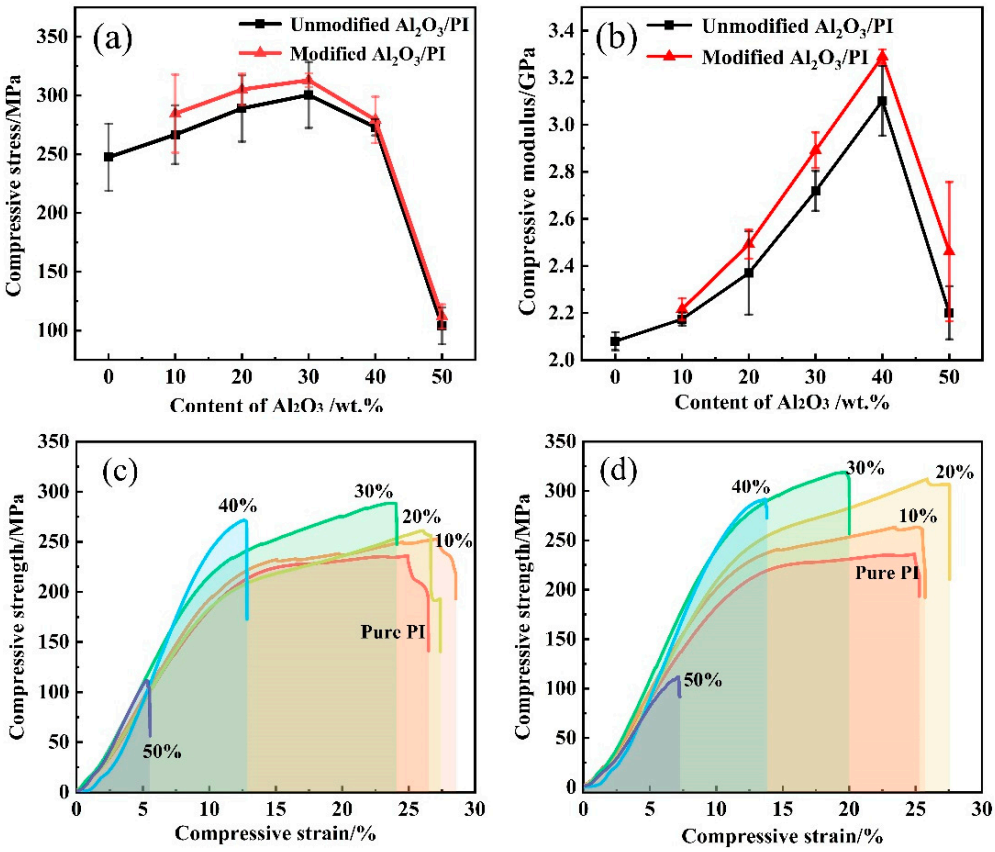

Figure 10. Compressive strength and modulus of PI/Al_2O_3 composites: (**a**) compressive strength; (**b**) compressive modulus; (**c**) stress–strain curve of composites with original Al_2O_3; (**d**) stress–strain curve of composites with modified Al_2O_3.

From the stress–strain curve shown in Figure 10c,d, it can be revealed that when the content of Al_2O_3 was below 20 wt.%, the strength of the composites increased slightly while maintaining good plasticity. When the content of Al_2O_3 reached 30 wt.%, the strength of the composite material was significantly improved, whereas the plasticity was reduced. The characteristic morphology of the fracture surface of PI/Al_2O_3 composites is demonstrated in Figure 11. As shown in Figure 11a, the fracture surface of pure PI was smooth and glassy; similar results can also be found in some previous studies [27–30]. The SEM images for 10 A-K and 30 A-K are shown in Figure 11b,c, respectively. It can be seen that the number of river-like cracks in pure polyimide reduced, and the roughness of the fracture surface increased with the increase of Al_2O_3 content. Table 2 shows the roughness values of the PI/Al_2O_3 nanocomposites and proves the increasing tread. For the sample of 10 A-K, the cracks propagated in a parabolic shape. In the case of 30 A-K, the roughness continued to increase, and some Al_2O_3 particles were well-dispersed throughout the polyimide matrix. However, after further increasing the content of Al_2O_3 powder, many pores or cracks, as well as agglomerates of nano-Al_2O_3, were clearly observed in the composite with 50 wt.% Al_2O_3, as shown in Figure 11d. The corresponding roughness also increased with an increase in the content of Al_2O_3.

Table 2. Roughness values of the PI/Al_2O_3 nanocomposites.

Samples	Roughness/μm
PI	0.995
10 A	1.176

Table 2. *Cont.*

Samples	Roughness/μm
20 A	1.596
30 A	2.111
40 A	2.424
50 A	3.058
10 A-K	1.680
20 A-K	1.986
30 A-K	2.492
40 A-K	2.542
50 A-K	3.207

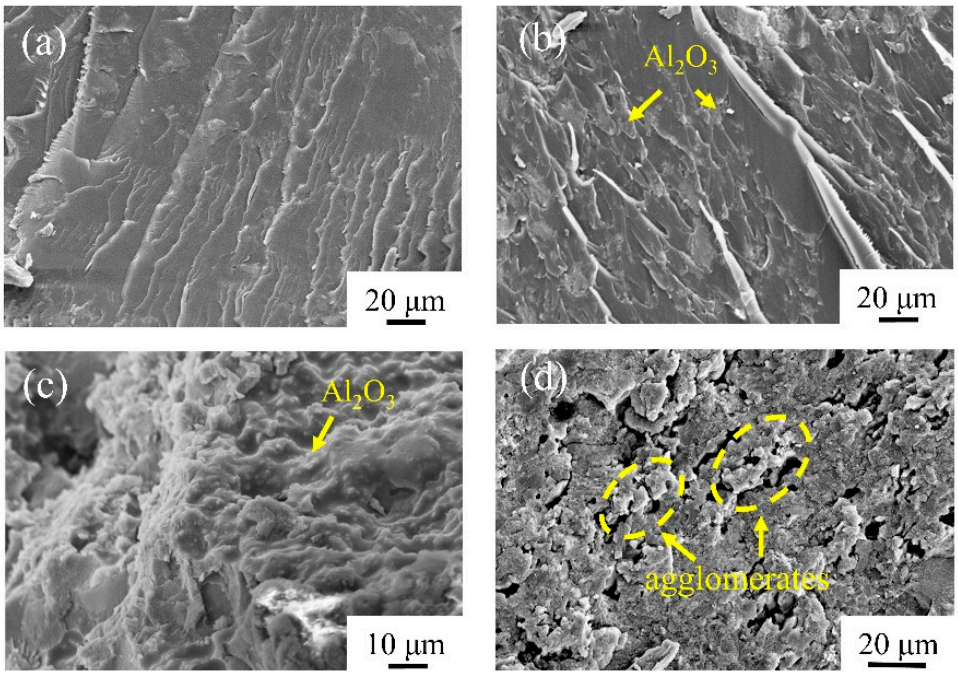

Figure 11. Characteristic morphology of fracture surface of PI/Al_2O_3 composites with different Al_2O_3 contents: (**a**) SEM image of pure PI; (**b**) SEM image of 10 A-K; (**c**) SEM image of 30 A-K; (**d**) SEM image of 50A.

4. Discussion

The thermosetting resin has weak crack propagation resistance, and the addition of inorganic nanoparticles is expected to improve the toughness of the polymer. An appropriate number of nano-sized powders can improve strength and modulus while ensuring good ductility. The cracks propagated at 45° in the pure PI sample, indicating the occurrence of shear deformation. However, it can only absorb a small amount of energy, while the excess energy will cause cracks to spread rapidly. When the content of Al_2O_3 was 10 wt.%, the cracks propagated in a parabolic shape, suggesting that the propagation path of the cracks was deflected. Additional energy input was required for the propagation of cracks. The propagation occurred locally by means of tensile and shear stresses, which induced an increase in the surface area of the fracture, leading to an increase in fracture toughness [31,32]. When the content of Al_2O_3 was less than 30 wt.%, the plasticity of the composite was maintained while the strength was increased.

There are three possible reinforcement mechanisms for the PI/Al_2O_3 composite. In one of the mechanisms, the reinforcement was due to the hydrolysis of silane coupling agents, which produce silicon–oxygen bonds and hydroxide ions. Silicon–oxygen bonds are very stable bonds in silane coupling agents, which can strongly adhere to the surface of inorganic materials. Aminopropyl groups at the other end can form hydrogen bonds

with polymers when cured [22,33,34]. Furthermore, the second reason is attributed to the transfer of shear stresses in the PI/Al_2O_3 interface, and the nanoparticle-matrix interaction is the major factor for its occurrence [35]. After the modification of nano-Al_2O_3, the bonding of the adsorption layer was enhanced. The appearance of -NH_2, -CH_2-, Si-C-H and Al-O-Si peaks in the FTIR spectrum and N and Si peaks in photoelectron spectra indicated that a modified layer was successfully prepared on the surface of nano-Al_2O_3, resulting in the improvement of strength and modulus. Another reinforcement effect was promoted through the formation of the three-dimensional network structure. During the crosslinking reactions, the PI chains were adsorbed to the surface of the nano-Al_2O_3 to form a local hardening zone, which reduced the mobility of the PI chains and enhanced the elastic modulus [36,37]. Figure 12 shows the schematic diagram of crack propagation in PI/Al_2O_3 composites. Under the action of external force, micro-cracks were generated in PI, molecular chains were broken, and the cracks propagated rapidly (see Figure 12a). It can be seen from Figure 12b that many Al_2O_3 particles were dispersed throughout the PI matrix. These Al_2O_3 particles can effectively hinder the propagation of the cracks, but parts of the particles were agglomerated in 30 A. After modification, the nano-Al_2O_3 particles were well-dispersed throughout the PI matrix (see Figure 12c); thus, the strength and modulus were further improved.

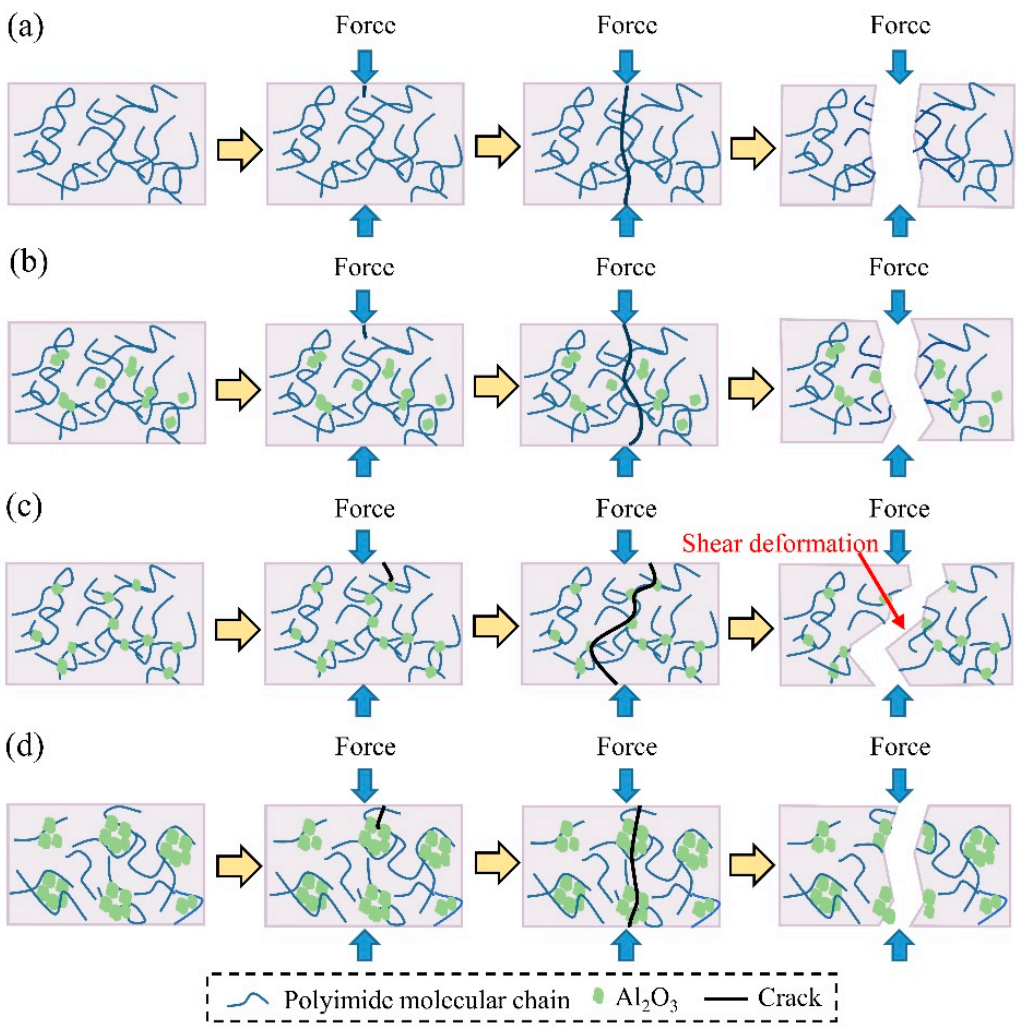

Figure 12. Schematic diagram of crack propagation in PI/Al_2O_3 composites: (**a**) pure PI; (**b**) composite with 30 wt.% original Al_2O_3 powder; (**c**) composite with 30 wt.% modified Al_2O_3 powder; (**d**) composite with 50 wt.% modified Al_2O_3 powder.

The strength of composites with a suitable content of nanoparticles was higher than that of pure PI matrix. For instance, Liu et al. [38] found that the PI/reduced graphene oxide (RGO)/Fe_2O_3 composites showed a compressive strength of 130.97 MPa and was 35.9% higher than pure PI. Zhao et al. [39] fabricated PI/nano-SiO_2 composites via an in situ polymerization method, in which the compressive strength of the composite with 5 wt.% nano-SiO_2 was 125.51 MPa, which increased by 42.6% compared to the pure PI with a compressive strength of 88.02 MPa. Compared to the above previous results, the compressive strength of PI/Al_2O_3 composites in this study was significantly improved. The compressive strength of 30 wt.% PI/Al_2O_3 can reach 313 MPa. However, as depicted in Figure 12d, when the content of nano-Al_2O_3 was too high, PI could not fill the gaps of agglomerates due to the agglomeration of excessive filler, leading to an increase in porosity and a decrease in strength. Additionally, the agglomeration of nano-Al_2O_3 easily caused the interfacial debonding of Al_2O_3 from the PI matrix, resulting in the initiation of cracks and stress concentration [40]. Therefore, the PI/Al_2O_3 composites with 30 wt.% modified Al_2O_3 exhibited the highest compressive strength.

5. Conclusions

In this study, a series of nano-Al_2O_3-reinforced polyimide (PI) composites were fabricated using the hot compression method. The thermal stability of the PI/Al_2O_3 composites was improved after the addition of Al_2O_3. The silane coupling agent was used to modify the surface of nano-Al_2O_3 to enhance the interface compatibility between Al_2O_3 and PI. The effects of Al_2O_3 contents on the microstructures and compressive properties of PI/Al_2O_3 composites were explored. Some main conclusions are as follows:

1. Chemical reactions occurred during the surface modification of nano-Al_2O_3. The appearance of -NH_2, -CH_2-, Si-C-H and Al-O-Si peaks in infrared spectroscopy and N and Si peaks in photoelectron spectra suggested that a modified layer was successfully prepared on the surface of Al_2O_3 nanoparticles.
2. Surface modification enhanced the interfacial compatibility between the Al_2O_3 and PI matrix. The compressive strength and compressive modulus of composites with modified Al_2O_3 were higher than those with original Al_2O_3 to some extent.
3. The compressive strength and compressive modulus of the composites initially increased and then decreased with the increase of Al_2O_3 content. The improvement of compressive properties of composites was due to the transfer of shear stresses in the nanoparticle–matrix interface and the formation of the three-dimensional network structure. When the Al_2O_3 content was 30 wt.%, the compressive strength of composites reached the maximum value of 313 MPa and increased by 26.5% compared to that of the PI matrix.

Author Contributions: Conceptualization, Y.B.; Methodology, Y.W.; Software, J.C. and B.W.; Validation, B.W.; Formal analysis, J.S.; Investigation, G.L. and Q.S.; Resources, G.M.; Data curation, J.C.; Writing—original draft preparation, J.C.; Writing—review and editing, Y.B., Y.W. and F.Y.; Visualization, Q.S.; Supervision, M.L.; Project administration, Y.W.; Funding acquisition, H.W. All authors have read and agreed to the published version of the manuscript.

Funding: This work was supported by the National Natural Science Foundation of China (Grant Nos. 52130509 and 52005388) and the Aviation Science Foundation of China (Grant No. 2023Z046070001).

Institutional Review Board Statement: Not applicable.

Informed Consent Statement: Not applicable.

Data Availability Statement: Data are contained within the article.

Conflicts of Interest: Author Guanghua Liu and Jian Sun were employed by the company China United Gas Turbine Technology Co., Ltd., Beijing 102209, China. The remaining authors declare that the research was conducted in the absence of any commercial or financial relationships that could be construed as a potential conflict of interest.

References

1. Wang, C.; Lan, Y.; Yu, W.; Li, X.; Qian, Y.; Liu, H. Preparation of amino-functionalized graphene oxide/polyimide composite films with improved mechanical, thermal and hydrophobic properties. *Appl. Surf. Sci.* **2016**, *362*, 11–19. [CrossRef]
2. Li, H.; Liu, G.; Liu, B.; Chen, W.; Chen, S. Dielectric properties of polyimide/Al_2O_3 hybrids synthesized by in-situ polymerization. *Mater. Lett.* **2007**, *61*, 1507–1511. [CrossRef]
3. Alias, A.; Ahmad, Z.; Ismail, A.B. Preparation of polyimide/Al_2O_3 composite films as improved solid dielectrics. *Mater. Sci. Eng. B* **2011**, *176*, 799–804. [CrossRef]
4. Liaw, D.-J.; Wang, K.-L.; Huang, Y.-C.; Lee, K.-R.; Lai, J.-Y.; Ha, C.-S. Advanced polyimide materials: Syntheses, physical properties and applications. *Prog. Polym. Sci.* **2012**, *37*, 907–974. [CrossRef]
5. Gouzman, I.; Grossman, E.; Verker, R.; Atar, N.; Bolker, A.; Eliaz, N. Advances in polyimide-based materials for space applications. *Adv. Mater.* **2019**, *31*, e1807738. [CrossRef] [PubMed]
6. Wang, H.; Ding, D.; Liu, Q.; Chen, Y.; Zhang, Q. Highly anisotropic thermally conductive polyimide composites via the alignment of boron nitride platelets. *Compos. Part B Eng.* **2019**, *158*, 311–318. [CrossRef]
7. Mekuria, T.D.; Wogsato, T.A. Synthesis, characterization and properties of polyimide nanocomposite thin films reinforced with TiO_2/Al_2O_3 hybrid nanoparticles. *Mater. Today Commun.* **2022**, *32*, 103903. [CrossRef]
8. Cai, H.; Yan, F.; Xue, Q.; Liu, W. Investigation of tribological properties of Al_2O_3-polyimide nanocomposites. *Polym. Test.* **2003**, *22*, 875–882. [CrossRef]
9. Dai, H.; Thostenson, E.T.; Schumacher, T. Comparative study of the thermoresistive behavior of carbon nanotube-based nanocomposites and multiscale hybrid composites. *Compos. Part B Eng.* **2021**, *222*, 109068. [CrossRef]
10. Malik, P.; Bhasha, B.; Jain, P. Influence of Surface modified Graphene Oxide on Mechanical and Thermal Properties of Epoxy Resin. *Orient. J. Chem.* **2018**, *34*, 1597–1603. [CrossRef]
11. Wang, X.; Jin, J.; Song, M. An investigation of the mechanism of graphene toughening epoxy. *Carbon* **2013**, *65*, 324–333. [CrossRef]
12. Singh, S.; Guchhait, P.K.; Bandyopadhyay, G.G.; Chaki, T.K. Development of polyimide–nanosilica filled EPDM based light rocket motor insulator compound: Influence of polyimide–nanosilica loading on thermal, ablation, and mechanical properties. *Compos. Part A Appl. Sci. Manuf.* **2013**, *44*, 8–15. [CrossRef]
13. Omar, M.F.; Akil, H.M.; Ahmad, Z.A. Mechanical properties of nanosilica/polypropylene composites under dynamic compression loading. *Polym. Composite.* **2011**, *32*, 565–575. [CrossRef]
14. Fu, S.; Sun, Z.; Huang, P.; Li, Y.; Hu, N. Some basic aspects of polymer nanocomposites: A critical review. *Nano Mater. Sci.* **2019**, *1*, 2–30. [CrossRef]
15. Tjong, S.C. Structural and mechanical properties of polymer nanocomposites. *Mat. Sci. Eng. R.* **2006**, *53*, 73–197. [CrossRef]
16. Fu, S.Y.; Feng, X.Q.; Lauke, B.; Mai, Y.W. Effects of particle size, particle/matrix interface adhesion and particle loading on mechanical properties of particulate–polymer composites. *Compos. Part B Eng.* **2008**, *39*, 933–961. [CrossRef]
17. Ning, N.; Wang, M.; Zhou, G.; Qiu, Y.; Wei, Y. Effect of polymer nanoparticle morphology on fracture toughness enhancement of carbon fiber reinforced epoxy composites. *Compos. Part B Eng.* **2022**, *234*, 109749. [CrossRef]
18. Maske, S.R.; Ganesh Gupta, K.B.N.V.S.; Kumar Prusty, R.; Ray, B.C. Effect of MWCNT/Nanosilica reinforcement on the mechanical and thermal behaviour of polymer composite. *Mater. Today Proc.* **2022**, *62*, 6087–6090. [CrossRef]
19. Zhang, H.; Tang, L.; Liu, G.; Zhang, D.; Zhou, L.; Zhang, Z. The effects of alumina nanofillers on mechanical properties of high-performance epoxy resin. *J. Nanosci. Nanotechnol.* **2010**, *10*, 7526–7532. [CrossRef]
20. Kango, S.; Kalia, S.; Celli, A.; Njuguna, J.; Habibi, Y.; Kumar, R. Surface modification of inorganic nanoparticles for development of organic–inorganic nanocomposites—A review. *Prog. Polym. Sci.* **2013**, *38*, 1232–1261. [CrossRef]
21. Belgacemi, R.; Derradji, M.; Trache, D.; Mouloud, A.; Zegaoui, A.; Mehelli, O.; Khiari, K. Effects of silane surface modified alumina nanoparticles on the mechanical, thermomechanical, and ballistic impact performances of epoxy/oxidized UHMWPE composites. *Polym. Composite.* **2020**, *41*, 4526–4537. [CrossRef]
22. Ahangaran, F.; Navarchian, A.H. Recent advances in chemical surface modification of metal oxide nanoparticles with silane coupling agents: A review. *Adv. Colloid Interface Sci.* **2020**, *286*, 102298. [CrossRef] [PubMed]
23. Duan, X.; Siew, W.H.; Given, M.; Liggat, J.; He, J. Effect of different surface treatment agents on the physical chemistry and electrical properties of polyethylene nano–alumina nanocomposites. *High Volt.* **2020**, *5*, 397–402. [CrossRef]
24. Tang, J.; Li, W.; Wang, Z. Facile synthesis of soluble, self-crosslinkable and crystalline polyimides with ultrahigh thermal/chemical resistance. *Polymer* **2023**, *268*, 125717. [CrossRef]
25. Nakamuraa, K.; Andoa, S.; Takeichi, T. Thermal analysis and solid-state ^{13}C NMR study of crosslink in polyimides containing acetylene groups in the main chain. *Polymer* **2001**, *42*, 4045–4054. [CrossRef]
26. Sezavar, A.; Zebarjad, S.; Sajjadi, S. A Study on the Effect of Nano Alumina Particles on Fracture Behavior of PMMA. *Technologies* **2015**, *3*, 94–102. [CrossRef]
27. Johnsen, B.B.; Kinloch, A.J.; Mohammed, R.D.; Taylor, A.C.; Sprenger, S. Toughening mechanisms of nanoparticle-modified epoxy polymers. *Polymer* **2007**, *48*, 530–541. [CrossRef]
28. Zhu, L.; You, L.; Shi, Z.; Song, H.; Li, S. An investigation on the graphitic carbon nitride reinforced polyimide composite and evaluation of its tribological properties. *J. Appl. Polym. Sci.* **2017**, *134*, 45403. [CrossRef]

29. Derradji, M.; Ramdani, N.; Zhang, T.; Wang, J.; Gong, L.D.; Xu, X.D.; Lin, Z.W.; Henniche, A.; Rahoma, H.K.S.; Liu, W.B. Thermal and mechanical properties enhancements obtained by reinforcing a bisphenol-a based phthalonitrile resin with silane surface-modified alumina nanoparticles. *Polym. Composite.* **2017**, *38*, 1549–1558. [CrossRef]
30. Zhang, P.; Bao, J.; Jiang, Z.; Dong, B.; Chen, X. Enhancing thermo-oxidative stability of thermoset polyimide composites using nano neodymium oxide particles. *J. Mater. Res. Technol.* **2021**, *14*, 2638–2649. [CrossRef]
31. Opelt, C.V.; Coelho, L.A.F. Reinforcement and toughening mechanisms in polymer nanocomposites—Reinforcement effectiveness and nanoclay nanocomposites. *Mater. Chem. Phys.* **2016**, *169*, 179–185. [CrossRef]
32. Opelt, C.V.; Becker, D.; Lepienski, C.M.; Coelho, L.A. Reinforcement and toughening mechanisms in polymer nanocomposites–Carbon nanotubes and aluminum oxide. *Compos. Part B Eng.* **2015**, *75*, 119–126. [CrossRef]
33. Ou, X.; Lu, X.; Chen, S.; Lu, Q. Thermal conductive hybrid polyimide with ultrahigh heat resistance, excellent mechanical properties and low coefficient of thermal expansion. *Eur. Polym. J.* **2019**, *122*, 109368. [CrossRef]
34. Mallakpour, S.; Dinari, M. Investigating the nanostructure and thermal properties of chiralpoly (amide-imide)/Al_2O_3 compatibilized with 3-aminopropyltriethoxysilane. *Mater. Res. Bull.* **2013**, *48*, 3865–3872. [CrossRef]
35. Yang, S.Y.; Lin, W.N.; Huang, Y.L.; Tien, H.W.; Wang, J.Y.; Ma, C.C.M.; Li, S.M.; Wang, Y.S. Synergetic effects of graphene platelets and carbon nanotubes on the mechanical and thermal properties of epoxy composites. *Carbon* **2011**, *49*, 793–803. [CrossRef]
36. Leong, Y.W.; Abu Bakar, M.B.; Ishak, Z.M.; Ariffin, A.; Pukanszky, B. Comparison of the mechanical properties and interfacial interactions between talc, kaolin, and calcium carbonate filled polypropylene composites. *J. Appl. Polym. Sci.* **2004**, *91*, 3315–3326. [CrossRef]
37. Bindu, P.; Thomas, S. Viscoelastic behavior and reinforcement mechanism in rubber nanocomposites in the vicinity of spherical nanoparticles. *J. Phys. Chem. B* **2013**, *117*, 12632–12648. [CrossRef]
38. Liu, H.; Jia, Y.; Wang, H.; Duan, C.; Wang, T.; Wang, Q. Ultra-high compression and wear resistant hybrid filled polyimide composite: Synergistic effect of Fe_2O_3 decorated RGO. *J. Appl. Polym. Sci.* **2020**, *137*, 49222. [CrossRef]
39. Zhao, Y.; Qi, X.; Dong, Y.; Ma, J.; Zhang, Q.; Song, L.; Yang, Y.; Yang, Q. Mechanical, thermal and tribological properties of polyimide/nano-SiO_2 composites synthesized using an in-situ polymerization. *Tribol. Int.* **2016**, *103*, 599–608. [CrossRef]
40. Idumah, C.I.; Obele, C.M. Understanding interfacial influence on properties of polymer nanocomposites. *Surf. Interfaces* **2021**, *22*, 100879. [CrossRef]